International Journal of Scientific & Engineering Research, Volume 14, Issue 9, September-2023
ISSN 2229-5518

Numerical Investigation of Cold-Formed Sigma Sections Subjected to Torsion

Ahmed Gamal, Ali Hammad, Sherif Ibrahim

Abstract— Cold-formed steel sections imposed itself as an economical construction material due it's high strength to weight ratio. The customizable nature of the cold-formed steel is an added advantage resulted in the ability to form numerous different geometries. Modifying the conventional Cee section geometry by adding intermediate stiffeners to the web resulted in forming a new geometry which has a superior behavior against the buckling instabilities. However, the slender and open nature of the conventional cold-formed geometries resulted in a significant susceptibility to twisting and warping stresses. The purpose of this paper is to investigate the behavior of cold-formed sigma sections when subjected to torsional stresses. These torsional stresses are induced by either the effect of the first-order eccentric loading or the effect of the second-order instabilities. First, a finite element model is verified against available experimental data. Then, the verified model is utilized for a wide range parametric study with torsional loading applied on a range of selected parameters including, geometries, steel grades, and member lengths. Finally, the ultimate bi-moment capacity is determined by performing a collapse analysis for the investigated models.

Index Terms— ABAQUS, Bi-moment, Cold-formed steel, CUFSM, Finite element analysis, Sigma sections, Warping.

1 Introduction

In modern construction industry cold-formed steel (CFS) is considered as low-priced material that could be used in many structural applications such as purlins and side rails. Sigma geometry is a modification to the conventional Cee geometry that resulted in Many advantages. One of these advantages is that the web stiffening brings the shear center closer to the C.G of the section and enhances the local and distortional behavior of the section. The geometrical change enhances the flexural behavior of the sigma sections when compared to the conventional Cee section. The shear center of many open CFS sections is outside the envelop of the geometry, so it is difficult to apply a transverse load without inducing torsional stresses. Inherently open CFS sections have low warping stiffness, thus these sections are susceptible to high twisting and warping. For the cases where torsional effects cannot be eliminated, the member has to be designed taking the torsional stresses into consideration. Current design codes AISI S100 [1], AS/NZS 4600 [2], Eurocode1-3 [3] and GB 50018[4] implemented provisions to account for the combined effect of torsional and flexural stresses. These provisions have some limitations, including addressing only the torsional first yield and ignoring the slenderness in torsion. Sigma section is not considered as a prequalified section; therefore, collapse analysis using finite element model is performed to obtain the nominal bi-moment capacity of the member and finite strip analysis is performed to obtain the critical buckling bi-moment.

- *Ahmed Gamal is currently pursuing masters degree program in structural engineering in Ain shams University, Egypt.*
- *Ali Hammad, Assistant Professor, Str. Eng. Dept. , Ain Shams university*
- *Sherif Ibrahim, Professor, Str. Eng. Dept. , Ain Shams university*

2 Literature Review

Torsional analysis of CFS first encountered when Bian et al. [5] carried out experimental and numerical investigation on Cee sections short beams under torsion only. Two sets of equations were provided as result of the study, moreover these equations considered the inelastic reserve behavior of the beams. Equation (1) described the behavior with parabolic inelastic reserve and and (2) is for the linear inelastic reserve.

$$\frac{T_n}{T_y} = f(x) = \begin{cases} 2 - \lambda_T^2, & \lambda_T \le 1 \\ 1/\lambda_T^2, & \lambda_T > 1 \end{cases} \quad (1)$$

$$\frac{T_n}{T_y} = f(x) = \begin{cases} 2.5 - 1.5\lambda_T, & \lambda_T \le 1 \\ 1/\lambda_T^2, & \lambda_T > 1 \end{cases} \quad (2)$$

where;T_n is torsional strength, T_y is torque at first yield and λ_t torsional slenderness $= (T_y/T_n)^{0.5}$.

Wan et al. [6] proved that the GB 50018 [4] see (3) is conservative by carrying out an experimental investigation on the torsional capacity of cee & zee sections subjected to combined bending and torsion stresses caused by changing the position of the load relative to the beam shear center. Cee section failed with section rotation & top flange distortional buckling. Zee section failed with section rotation, top flange distortional buckling and local buckling in the bottom flange. Fig.1 shows the used test set up.

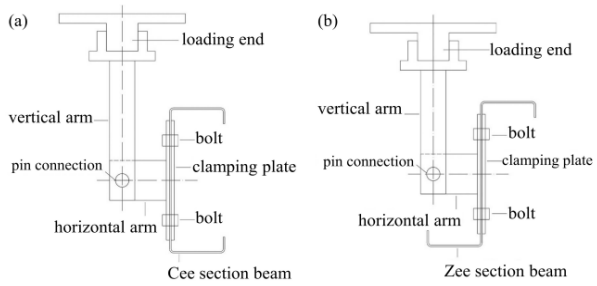

Fig. 1 The test setup to apply the torsional loading (a) Cee section, (b) ZEE section

$$\frac{M}{M_b} + \frac{B}{B_y} \leq 1 \quad (3)$$

where; M_b is bending capacity under bending moment only and B_y is bi-moment capacity under torsion only.

Xia et al. [7] developed a simple method to predict the bi-moment capacity of cold-formed Cee sections by developing a set of parameters, including yield bi-moment B_y, plastic bi-moment B_p, buckling bi-moment B_{cr}, and bi-moment strength B_n see (4).

$$\frac{B_n}{B_{cr}} = \frac{B_{cr}+aB_y}{B_{cr}+bB_y} = \frac{1+a\lambda_B^2}{1+b\lambda_B^2} \quad (4)$$

(a) and (b) were iterated and determined in the regression analysis by finding the optimal fit between the simulation data and the predicted data on the other hand λ_B is the slenderness for bi-moment see (5).

$$\lambda_B = \left(T_y/T_n\right)^{0.5} \quad (5)$$

AISI S100 (2020) [1] "Section H4" Indicates that flexural strength of cold-formed sections subjected to combined flexural and torsional stresses shall be reduced by a factor called "R" as shown in (6).

$$R = \frac{f_{bending\ max}}{f_{bending} + f_{bending\ torsion}} \quad (6)$$

where; $f_{bending\ max}$ is bending stress at the extreme fiber, $f_{bending}$ is bending stress at location where combined torsion and bending stresses are maximum in the cross-section and $f_{bending\ torsion}$ is torsional warping stress at location where combined torsion and bending stresses are maximum in the cross-section.

Eurocode-3- Part 1-3 [3] Considers the torsion effect due to eccentric loading by using specific conditions which must be satisfied, see (7).

$$\sqrt{\sigma_{tot,Ed}^2 + 3.\tau_{tot,Ed}^2} \leq \frac{1.1 f_y}{\gamma_{Mo}} \quad (7)$$

where; $\sigma_{tot,Ed}$ is total longitudinal stresses, calculated on the relevant effective cross- section, $\tau_{tot,Ed}$ is total shear stress, calculated on the gross cross-section γ_{Mo} is safety factor.

The purpose of this paper is to use the available leturature to develop a finite strip model which will be used to capture the critical buckling mode of the section then a finite element model will be developed to obtain the internal bi-moment capacity of the section and a comparison between the yield bi-moment, plastic bi-moment, critical buckling bi-moment and the internal bi-moment capacity will be shown in tabulated form.

3 VERIFICATION

This stage is intended to verify the numerical model against the experimental data presented in Wan et al. [6]. The experiment investigated the behavior of CFS setions when subjected to combined torsional and flexural loading.

3.1 Element Type

The cold-formed Cee section is simulated using a four-node shell element having five degrees of freedom, including three translation and two in-plane rotations (rotation around the shell normal is excluded to reduce the analysis time). This shell element type is defined in ABAQUS CAE [8] software as S4R5 shell. This shell element type is suitable to analyze CFS sections and also permits including of both material and geometric non-linearity. The elements have an aspect ratio between 0.5 and 2 as recommended by Xia et al [7].

3.2 Loading, Test Set-up, and Boundary Conditions

The beam testing in Wan et al. [6] is done by applying a concentrated eccentric load at the middle span of the tested beam. This load was applied outside the beam web through a special rig. This rig is designed to transmit the vertical load with varies range of eccentricities. The load was applied through the vertical arm while the eccentricity value is controlled using the horizontal arm. Fig.1 shows the test setup as per Wan et al. [6]. To ensure that the beam could rotate freely during the test the vertical and horizontal arms are pinned. The flexural loading is introduced by the vertical load while the torsional load is introduced by the different eccentricities. Each end of the beam is held inside the supports, their vertical displacement, lateral displacement and rotations are fully restrained. The beam ends are held by top and bottom rollers to allow for free bending in the vertical plane and free warping in the longitudinal direction. Fig.2 presents a schematic of the end supports. The experimental data included testing two different geometries for Cee section (180X70X20X2.5 and 185X70X20X1.8) the naming of the test specimen is following the form DxBxdxt, Where D, B and d are the outer-to-outer depth, flange width, and lip length, t is the specimen wall thickness. Two different steel grades are introduced, each associated with specific wall thickness. For t = 2.5 mm steel is 345 Mpa and for t = 1.8 mm steel is 318 Mpa. Based on the fact that the torsional effect is more significant when the torsional loading is applied to short spans. Two short spans are investigated (1200 mm and 1500 mm). Three different eccentricities are introduced to each case (30, 40 and 50 mm). The geometric characteristics of the modelled beam are illustrated in Table 1.

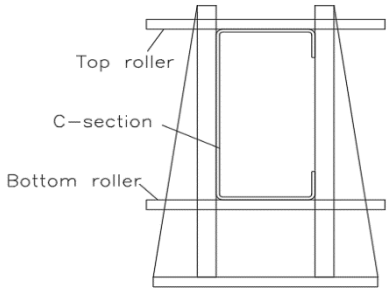

Fig. 2 Schematic drawing of beam end support

TABLE 1

Section	D X B X d X t	span L (mm)	Eccentricity e (mm)
C-section	180x70x20x2.5	1200	30
	180x70x20x2.5	1200	40
	180x70x20x2.5	1200	50
	180x70x20x2.5	1500	30
	180x70x20x2.5	1500	40
	180x70x20x2.5	1500	50
	185x70x20x1.8	1200	30
	185x70x20x1.8	1200	40
	185x70x20x1.8	1200	50
	185x70x20x1.8	1500	30
	185x70x20x1.8	1500	40
	185x70x20x1.8	1500	50

The finite element model included vertical load "P" applied at the mid span. This vertical load is directly acting on the web, top flange junction. The torsional load is introduced by a pair of horizonal loads "Q" acting on the upper and lower web to flange junction and this load is calculated using (8). where "ds" is the distance between the shear center and the beam web center and "e" is the eccentricity applied using the horizontal arm Fig. 3 shows the applied vertical and horizontal loads.

$$Q = P(Ds + e)/D \quad (8)$$

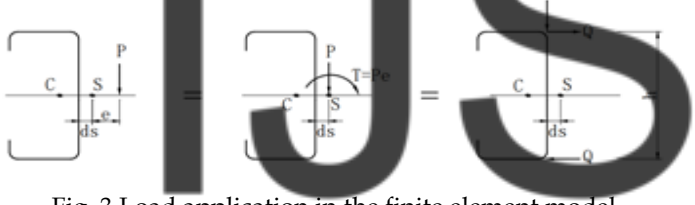

Fig. 3 Load application in the finite element model

Boundary conditions are applied to the beam ends to ensure that the nodes are restrained in the section plane, thus the rotation about the longitudinal directions is restrained. To ensure the validation of the warping free assumption the nodes at the two ends of the beam are free to move in the longitudinal direction. To prevent rigid body motion the nodes at the middle span cross section are restrained against longitudinal movement. Illustration of the modelled beam boundary condition is shown in Fig. 4.

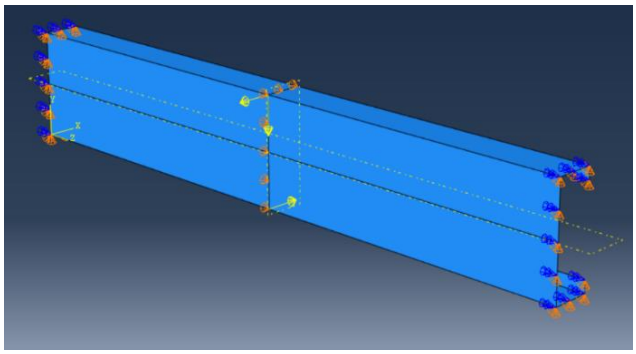

Fig. 4 Finite element model boundary conditions and loading

3.3 Material property

The material is modeled using elastic perfectly plastic (EPP) stress strain curve. Poisson's ratio, v, is assumed to be 0.3 and the modulus of elasticity, E, is assumed to be 203 N/mm^2 as recommended by Xia et al. [7].

3.4 Geometric imperfections

Simulation of the finite element model to understand the effect of geometric imperfections (GI) is developed by simulating two models, one with geometric imperfections and the other without geometric imperfections.

3.5 Finite element verification results

Comparison between test results and collapse analysis is performed and presented in Fig. 5. The comparison reveals a good agreement between finite element results and the test results available in Wan et al. [6]. See Table 2 for details. The relations between the load and the flanges lateral displacement from the finite element analysis and the experimental data are illustrated in (Fig. 6 to Fig. 11).

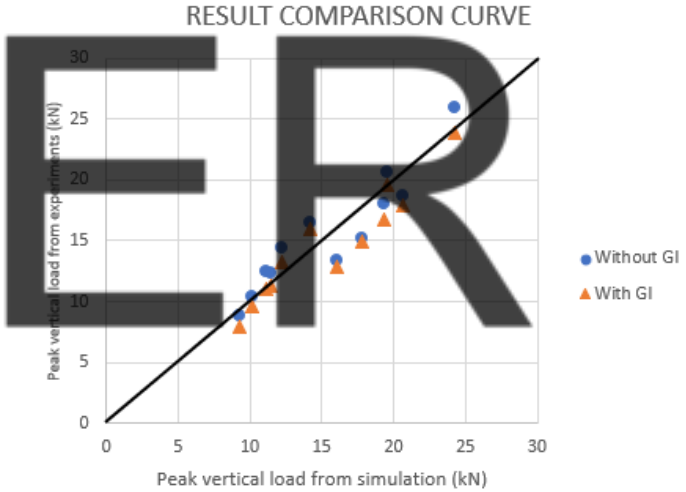

Fig. 5 Comparison between the experimental results and the finite element

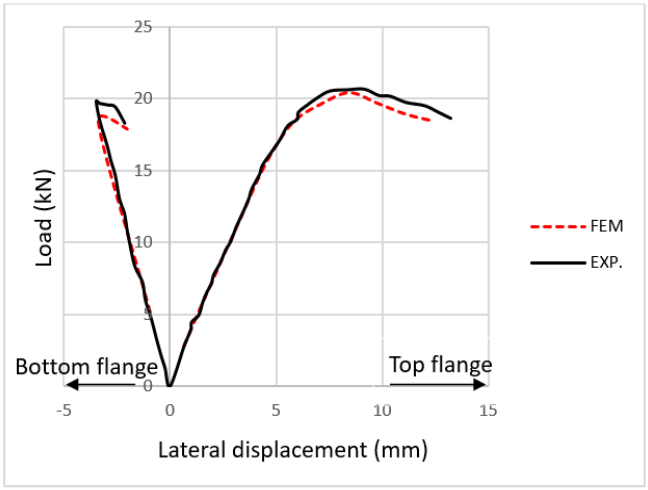

Fig. 6 Top and Bottom flanges lateral displacement for C180x70x20x2.5, L=1500 and e = 30 mm

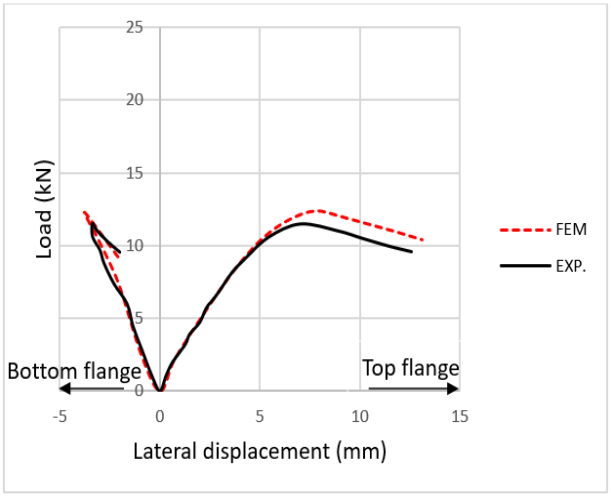

Fig. 9 Top and Bottom flanges lateral displacement for C185x70x20x1.8, L=1500 and e = 30 mm

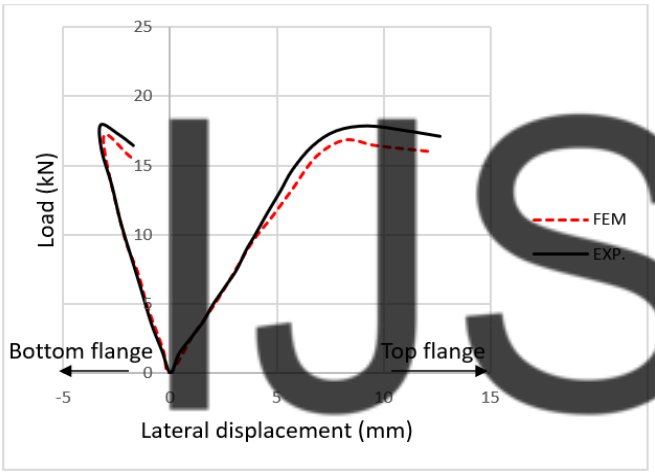

Fig. 7 Top and Bottom flanges lateral displacement for C180x70x20x2.5, L=1500 and e = 40 mm

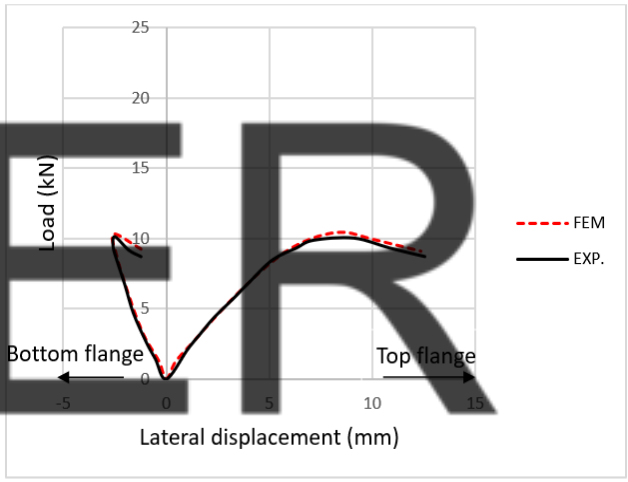

Fig. 10 Top and Bottom flanges lateral displacement for C185x70x20x1.8, L=1500 and e = 40 mm

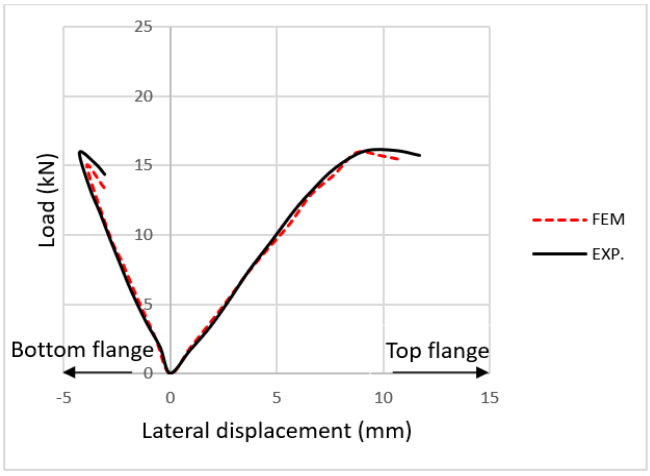

Fig. 8 Top and Bottom flanges lateral displacement for C180x70x20x2.5, L=1500 and e = 50 mm

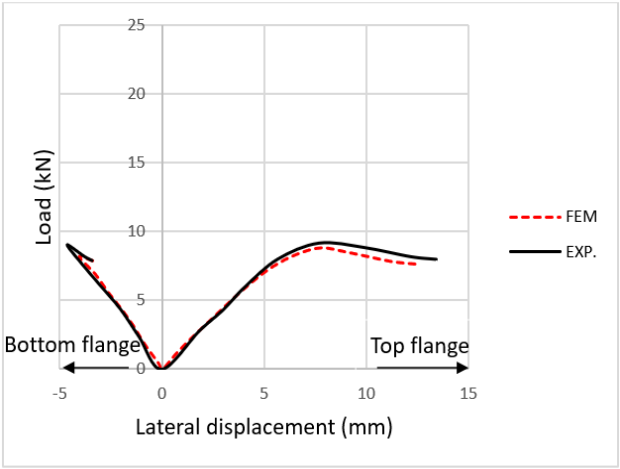

Fig. 11 Top and Bottom flanges lateral displacement for C185x70x20x1.8, L=1500 and e = 50 mm

TABLE 2

section	D x B x d x t	span L (mm)	Eccentricity e (mm)	EXP. Ultimate load (kN)	FEA (without initial imperfection)		FEA (with initial imperfection)	
C-section	180x70x20x2.5	1200	30	24.3	25.94	0.9367	23.91	1.0163
		1200	40	19.59	20.59	0.9514	19.63	0.9979
		1200	50	19.37	18.04	1.0737	16.81	1.1522
		1500	30	20.68	18.66	1.1082	17.96	1.1514
		1500	40	17.84	15.2	1.1736	14.9	1.1973
		1500	50	16.1	13.4	1.2014	12.86	1.25194
	185x70x20x1.8	1200	30	14.18	16.52	0.8583	16.03	0.8845
		1200	40	12.19	14.42	0.8453	13.3	0.9165
		1200	50	11.08	12.45	0.8899	11.02	1.0054
		1500	30	11.42	12.34	0.9254	11.3	1.0106
		1500	40	10.16	10.39	0.9778	9.6	1.0583
		1500	50	9.27	8.84	1.0486	7.91	1.1719
MEAN						0.9992		1.0678
STANDARD DEVIATION						0.1201		0.1155

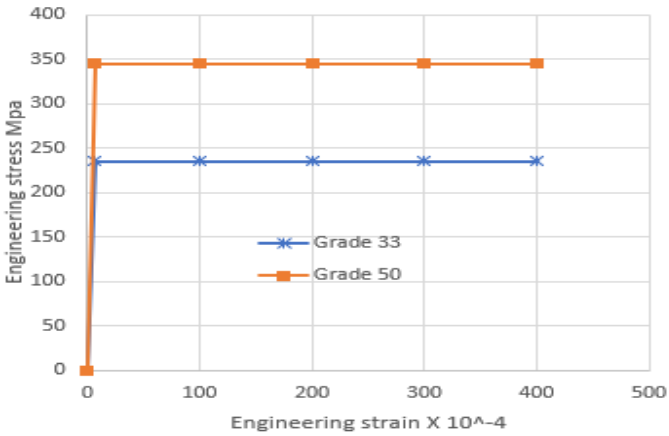

Fig. 13 Stress-Strain curve for the used materials

4 PARAMETRIC STUDY

4.1 Parametric study simulation data

The aim of this study is to investigate the torsional bi-moment behavior, so to develop a case with pure torsional bi-moment at mid span the verified finite element model is adjusted by removing the vertical load "P" which was used to introduce bending to the section and convert the concentrated torsional load "Q" introduced early at the verification to a distributed load along the beam span, where the value of the distributed torsion "q = Q / L" and "L" is the member span. illustration of the modified finite element model is shown in Fig. 12. Two types of steel grades are used in the parametric study, including both (ASTM A653, SS Grade 33) and (ASTM A653, SS Grade 50). The stress strain curve for each steel is shown in Fig. 13.

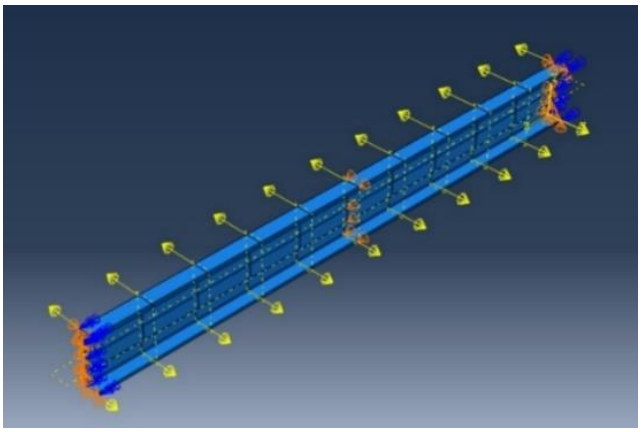

Fig. 12 Finite element model boundary conditions and loading

The initial geometric imperfection shapes for both local and distortional buckling cases when the member is subjected to bi-moment only are determined by using finite strip analysis (see Fig. 14). The maximum imperfections amplitude is adopted same as discussed in section (3.4). As stated by Xia et al. [7] The average difference in bi-moment capacity between the with and without geometric imperfections cases is within 1 %.

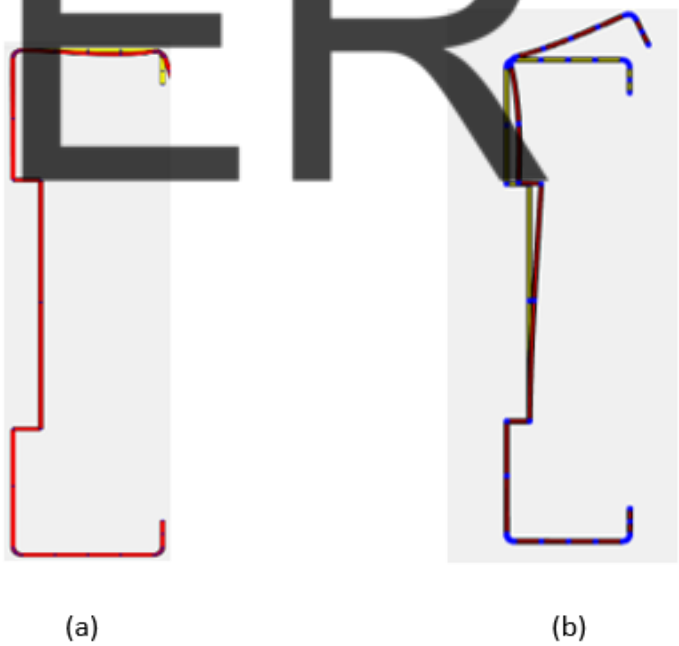

Fig. 14 Intial geometric imperfections (a) local buckling, (b) distortional buckling.

Twenty different cross section sizes are used as shown in Table 3. As recommended by Xia et al. [7] no need to simulate the beam under opposite torsional moment direction, as the results are almost the same for both the clockwise and the counter-clockwise cases.

TABLE 3

ID	D mm	F mm	t mm	L mm	R mm	S mm	O mm
1600Σ350x97	406.4	88.9	2.58318	25.4	3.8735	16	101.6
1600Σ350x68	406.4	88.9	1.81102	25.4	2.71526	16	101.6
1400Σ350x97	355.6	88.9	2.58318	25.4	3.8735	16	88.9
1400Σ350x68	355.6	88.9	1.81102	25.4	2.71526	16	88.9
1400Σ350x54	355.6	88.9	1.43764	25.4	2.15646	16	88.9
1200Σ300x97	304.8	76.2	2.58318	15.875	3.8735	16	76.2
1200Σ300x68	304.8	76.2	1.81102	15.875	2.71526	16	76.2
1200Σ300x54	304.8	76.2	1.43764	15.875	2.15646	16	76.2
1000Σ300x97	254	76.2	2.58318	15.875	3.8735	16	60.96
1000Σ300x68	254	76.2	1.81102	15.875	2.71526	16	60.96
1000Σ300x54	254	76.2	1.43764	15.875	2.15646	16	60.96
800Σ250x97	203.2	63.5	2.58318	15.875	3.8735	16	50.8
800Σ250x68	203.2	63.5	1.81102	15.875	2.71526	16	50.8
800Σ250x54	203.2	63.5	1.43764	15.875	2.15646	16	50.8
600Σ250x97	152.4	63.5	2.58318	15.875	3.8735	16	38.1
600Σ250x68	152.4	63.5	1.81102	15.875	2.71526	16	38.1
600Σ250x54	152.4	63.5	1.43764	15.875	2.15646	16	38.1
600Σ200x97	152.4	50.8	2.58318	15.875	3.8735	16	38.1
600Σ200x68	152.4	50.8	1.81102	15.875	2.71526	16	38.1
600Σ200x54	152.4	50.8	1.43764	15.875	2.15646	16	38.1

The internal ultimate bi-moment "$B_{n\sigma}$ " at mid span is calculated from the nodal longitudinal stresses when peak "q" is captured as presented in (9).

$$B_{n\sigma} = \int \sigma \, W_n \, dA \quad (9)$$

4.2 Results and discussion

Finite strip analysis was performed to capture the critical buckling mode of the sections. The analysis shows that the sections critical buckling is controlled by the distortional buckling mode. Finite element analysis was performed to obtain the internal bi-moment capacity of the beams $B_{n\sigma}$, see Table 4 for details. Results show that the value of $B_{n\sigma}$ is between B_y and B_{crd} Additionally $B_{n\sigma}$ is smaller than B_p for all cases. B_y is the yield bi-moment, B_p is the plastic bi-moment, B_{crd} is the critical distortional buckling bi-moment.

TABLE 4

Section	Type	Bp	By	B_{cr}	$B_{n\sigma}$
1600Σ350x97	Gr50	2.506	1.253	2.8568	1.647
1600Σ350x68	Gr50	1.7535	0.9086	1.3810	1.011
1400Σ350x97	Gr50	1.9789	1.056	2.4816	1.269
1400Σ350x68	Gr50	1.3789	0.7661	1.2027	0.828
1400Σ350x54	Gr50	1.0928	0.6178	0.7537	0.587
1200Σ300x97	Gr50	1.2936	0.588	1.3524	0.873
1200Σ300x68	Gr50	0.9007	0.431	0.6465	0.493
1200Σ300x54	Gr50	0.7143	0.3493	0.4016	0.369
1000Σ300x97	Gr50	0.9481	0.4648	1.1155	0.815
1000Σ300x68	Gr50	0.6577	0.3408	0.5316	0.375
1000Σ300x54	Gr50	0.5222	0.2763	0.3343	0.275
800Σ250x97	Gr50	0.5282	0.2723	0.9285	0.476
800Σ250x68	Gr50	0.3674	0.2008	0.4477	0.257
800Σ250x54	Gr50	0.2909	0.1632	0.2807	0.173
600Σ250x97	Gr50	0.3225	0.1854	0.6915	0.323
600Σ250x68	Gr50	0.2256	0.137	0.3356	0.1807
600Σ250x54	Gr50	0.1782	0.1114	0.2105	0.123
600Σ200x97	Gr50	0.2571	0.1405	0.7390	0.2567
600Σ200x68	Gr50	0.1776	0.1045	0.3563	0.163
600Σ200x54	Gr50	0.1402	0.085	0.2244	0.1085
1600Σ350x97	Gr33	1.6494	0.8247	2.8617	1.28
1600Σ350x68	Gr33	1.1537	0.5978	1.3809	0.666
1400Σ350x97	Gr33	1.3029	0.6953	2.4891	1.1
1400Σ350x68	Gr33	0.9072	0.504	1.1995	0.6
1400Σ350x54	Gr33	0.7190	0.4065	0.7520	0.428
1200Σ300x97	Gr33	0.8511	0.3869	1.3541	0.6407
1200Σ300x68	Gr33	0.5927	0.2836	0.6466	0.365
1200Σ300x54	Gr33	0.4699	0.2298	0.4021	0.2475
1000Σ300x97	Gr33	0.6238	0.3058	1.1161	0.6123
1000Σ300x68	Gr33	0.4327	0.2242	0.5335	0.292
1000Σ300x54	Gr33	0.3436	0.1818	0.3326	0.1965
800Σ250x97	Gr33	0.3476	0.1792	0.9300	0.36
800Σ250x68	Gr33	0.2417	0.1321	0.4478	0.199
800Σ250x54	Gr33	0.1914	0.1074	0.2813	0.137
600Σ250x97	Gr33	0.2122	0.122	0.6917	0.2584
600Σ250x68	Gr33	0.1483	0.0901	0.3351	0.1427
600Σ250x54	Gr33	0.1172	0.0733	0.2103	0.0988
600Σ200x97	Gr33	0.1690	0.0924	0.7382	0.19
600Σ200x68	Gr33	0.1167	0.0687	0.3558	0.1215
600Σ200x54	Gr33	0.0924	0.056	0.2245	0.0853

5 Conclusion

In this paper, an illustration of the literature on torsional analysis of CFS has been presented. Verification of the FEM against the available test data is carried out. Wide range parametric study is conducted using the verified FEM. Geometric imperfections, material grade, stress strain behavior, direction of the torsional moment, buckling, and wide range of cross section sizes are the main parameters considered in the study. Additional future work on developing reliable equations describing the torsional behavior of CFS open sections considering various boundary conditions is a priority.

References

[1] American Iron and Steel Institute (2020). S100-16 (R2020): North American Specification for the Design of Cold-formed Steel Structural Members. Washington, DC, U.S.A.
[2] AS/NZS Australian / New Zealand Standard TM, Australian / New Zealand Standard TM Cold-formed steel structures 4600:2005, ‖ vol. 2005, no. 1, p. 153, 2005.
[3] European Committee for Standardization (CEN) (2006). Eurocode 3: Design of steel structures, Part 1-3: General rules - Supplementary rules for cold-formed members and sheeting. Brussels, Belgium, pp. 1–130.
[4] Ministry of Construction of the P.R.C and General Administration of Quality Supervision, In section and Quarantine of the P.R.C (2002). Technical code of cold-formed thin-wall steel structures. Beijing, China, pp. 1–93.
[5] Bian, Guanbo et al. (2016). "Torsion of cold-formed steel lipped channels dominated by warping response". In: Thin-Walled Structures 98, pp. 565–577.
[6] Wan, Hong Xia, Bin Huang, and Mahen Mahendran (2021). "Experiments and numerical modelling of cold-formed steel beams under bending and torsion". In: Thin-Walled Structures 161, p. 107424. ISSN: 02638231. DOI: 10.1016/j.tws.2020.107424.
[7] Xia, Yu et al. (2022). Cold-formed steel strength predictions for torsion. Proceedings of the annual stability conference. Structural stability research council Denver, Colorado, March 22-25,2022.
[8] Abaqus (2016). Version 6.16 Dassault Systemes Simulia Corp.